The Astrophysical Journal Letters, 900:L17 (7pp), 2020 September 10 https://doi.org/10.3847/2041-8213/abb096

Localized Amplification of Magnetic Field in the Solar Photosphere Associated with a Rapid Moving Pore

Zhe Xu[1,2,3], Haisheng Ji[1,3], Kaifan Ji[2,3], Yi Bi[2,3], Bo Yang[2,3], Junchao Hong[2,3], and Jiayan Yang[2,3]
[1] Purple Mountain Observatory, Chinese Academy of Sciences, No.8 Yuanhua Road, Qixia District, Nanjing 210034, People's Republic of China; xuzhe@pmo.ac.cn
[2] Yunnan Observatories, Chinese Academy of Sciences, 396 Yangfangwang, Guandu District, Kunming 650216, People's Republic of China
[3] Center for Astronomical Mega-Science, Chinese Academy of Sciences, 20A Datun Road, Chaoyang District, Beijing 100012, People's Republic of China
Received 2020 May 20; revised 2020 August 17; accepted 2020 August 17; published 2020 September 3

Abstract

In the Sun, the flows of hot plasma drive a dynamo that generates a global magnetic field as well as smaller-scale local fields. The existence of a magnetic field in turn affects the motion of plasma so that complex dynamic characteristics can be observed. In this Letter, we give an analysis on the localized amplification of magnetic fields in front of a moving pore. Moving with the pore, the formation of semicircular penumbra-like structures and enhancement of horizontal fields can be observed simultaneously. The increasing horizontal magnetic fields in a penumbra-like area probably did not come from the pore, since the penumbra-like structures were not connected to the pore and a magnetic gap existed. The possibility of flux emergence can also be safely excluded. We further report that horizontal magnetic fields in the front of a moving pore are amplified in accordance with the MHD induction equation after necessary yet reasonable simplification. All characteristics show that the flows driven by the moving pore can lead to the amplification of the magnetic fields around its front. The observations are from the Helioseismic and Magnetic Imager on board the Solar Dynamics Observatory.

Unified Astronomy Thesaurus concepts: Solar magnetic fields (1503); Solar photosphere (1518); Sunspot flow (1978); Penumbra (1205); Solar dynamo (2001); Sunspots (1653); Solar active regions (1974); Solar active region velocity fields (1976)

1. Introduction

Since Hale detected magnetic fields on the Sun more than a century ago (Hale 1908), the generation of magnetic fields on stars has been a long-standing hot topic in natural science (Parker 1955; Babcock 1961; Leighton 1969; Parker 1970; Brandenburg et al. 1996). For large-scale magnetic features like sunspots, they are believed to be produced by the global dynamo, operating in the solar convection zone through the shear flows made by differential rotation and helical turbulent motion (Ribes et al. 1985; Rempel & Schlichenmaier 2011; Brandenburg et al. 2012; Charbonneau 2014; Jiang et al. 2014; Cameron et al. 2017; Kumar et al. 2019). Within this framework, recent solar cycles have been successfully predicted. For small-scale magnetic features like the internetwork fields and other magnetic carpets of ephemeral regions, their origin is still a problem. A widely used scenario is the so-called local dynamo operated by the interaction between the near-surface turbulent flows and ambient magnetic fields (Golub et al. 1981; Brandenburg 2005; Brandenburg et al. 2012; Kitiashvili et al. 2015; Käpylä et al. 2018; Rempel 2018) on the scale of a granulation (Cattaneo 1999; Vögler & Schüssler 2007). The local dynamo is difficult to directly observe, mainly due to the fact that we still do not have sufficient spatial resolution and polarimetry precision to resolve velocity and magnetic fields of a solar granulation. However, horizontal proper motions of large-scale magnetic features and associated horizontal plasma velocities have been reported recently (Verma et al. 2016; Ermolli et al. 2017). If these detectable magnetic fields and plasma flows can interact and amplify the localized magnetic field is a question worthy of study.

Here, by using the observations from the Helioseismic and Magnetic Imager (HMI; Schou et al. 2012) on board the Solar Dynamics Observatory (SDO; Pesnell et al. 2012), we give an analysis of observed localized amplification of magnetic fields in the front of a pore (sunspot with naked umbra) that undergoes a rapid proper motion after many complex evolving processes including magnetic cancellation. This pore moves sufficiently fast and takes its passage inside a very weak background magnetic field. It therefore provides us an excellent astronomical MHD experiment to investigate the interaction between the magnetic field and its ambient plasma flows. After both observations and theoretical estimation, our research suggests that the flows driven by the moving pore could lead to the amplification of the magnetic fields around its front.

2. Observations and Data Processing

The evolution of the target pore during its rapid moving passage was well recorded by the observations from HMI on board SDO. HMI takes full-disk continuum intensity images and Dopplergrams with a pixel size of 0.″5 and a 45 s cadence. HMI also provides the vector magnetograms of Space weather HMI Active Region Patches (SHARPs; Turmon et al. 2010), which have a 12 minute cadence and an accuracy of ∼10 G/∼100 G for the vertical/horizontal component. The vector field data have been remapped to a Lambert cylindrical equal area projection (Bobra et al. 2014), and then transformed into standard heliographic spherical coordinates to match the HMI continuum intensity images. Interface Region Imaging Spectrograph (IRIS; de Pontieu et al. 2014) 2832 Å images are also available, with a pixel size of 0.″33 and 37 s cadence.

All of the above data are rotated to a reference time at 22:00 UT on 2016 May 15.

The photospheric velocity fields are derived by applying the Differential Affine Velocity Estimator for Vector Magnetograms (DAVE4VM; Schuck 2008) on the HMI vector magnetic fields. The window size is set to 10 pixels, which provides a spatial resolution of 5″ for us to investigate the magnetic features in this event. The velocity fields are further corrected by removing the irrelevant field-aligned plasma flow using

$$\boldsymbol{V}_{\perp} = \boldsymbol{V} - \frac{\boldsymbol{V}\cdot\boldsymbol{B}}{B^2}\boldsymbol{B}, \tag{1}$$

where $\boldsymbol{V}$ is the velocity derived by DAVE4VM, and $\boldsymbol{V}_{\perp}$ is the velocity perpendicular to the magnetic field line that can denote the transport velocity of the magnetic flux in the photosphere (Kusano et al. 2002; Liu & Schuck 2012). $\boldsymbol{V}_{\perp}$ can be decomposed into $\boldsymbol{V}_{\perp_n}$ and $\boldsymbol{V}_{\perp_t}$, which are in the directions of normal and tangential to the solar surface, respectively. The $\boldsymbol{V}_{\perp_n}$ term is related to the emergence or the submergence, and $\boldsymbol{V}_{\perp_t}$ is related to the shear motion on the surface. Here, $\boldsymbol{V}_{\perp_t}$ is adopted as the photospheric flow field $\boldsymbol{u}\,(u_x, u_y)$ to estimate the amplification of the horizontal magnetic fields produced by the shear flows in the photosphere.

3. Results

3.1. Overview of the Rapid Moving Pore in AR 12544

NOAA active region (AR) 12544 (also named as HARP 6550) studied here was located near the central meridian (N21W15) on 2016 May 15. The region shows a typical βp configuration, with sunspots dominant in the preceding but scattered in the following part as shown in Figures 1(a), (b). The target negative pore is highlighted by the blue arrow, which initially was located around the middle of the AR. The pore moved straight forward, and finally merged into the leading sunspot as illustrated by its trajectory (green curve) overplotted in Figure 1(b). Semicircular penumbra-like structures are formed at the moving front of the pore as presented in the close-up views of the HMI intensitygrams (Figures 1(c1)–(c3), also see the animation of Figure 1). These structures are unstable and definitely are not a penumbra as usually regarded, since they are not connected to the pore as clearly shown by the IRIS 2832 Å image (Figure 1(d)) with a higher spatial resolution.

To detail the whole moving course, Figure 1(e) shows the time profile of the displacement of the pore by tracking its centroid for 14 hr. It can be seen that, after a very short acceleration, the pore moves with a nearly constant speed ($\sim$0.91 km s^{-1}). Such a movement is maintained for about 5 hr until it gradually slowed down and eventually merged into the preceding spots. Accordingly, the whole moving course can be divided into two phases, the rapid moving phase and the decelerating phase, which was roughly separated by the time at around 00:45 UT of 2016 May 16. The semicircular penumbra-like structures mainly occurred during the rapid moving phase, and they gradually disappeared in the following decelerating phase. Hence, the formation of these ephemeral structures is closely associated with the rapid proper motion of the pore as implied by the observations.

3.2. Magnetic Field, Electric Current, and Lorentz Force

Figure 2 shows our diagnosis of the magnetic field of the pore and penumbra-like structures. Here, the horizontal magnetic field in rectangular coordinates ($\boldsymbol{B}_{x,y}$) has been transformed into polar coordinates ($\boldsymbol{B}_{r,\theta}$) to better investigate the semicircular features. First, there is a very obvious magnetic gap (at $r \sim 2\farcs2$) between the pore and penumbra-like structures, as shown by each component of the magnetic field strength in Figure 2(b) and the magnetic field inclination in Figure 2(c). It is very different from a typical sunspot, where the change rate of the magnetic field is nearly continuous at the boundary between the umbra and the penumbra (see the examples in Borrero & Ichimoto (2011); Jurčák (2011); Murabito et al. (2016)). Second, in the penumbra-like area ($2\farcs2 < r < 6\farcs2$), the vertical field B_z and radial field B_r are fairly weak, similar to those of convective granule areas ($r > 6\farcs2$), while azimuthal field B_θ is very strong and decreases from $\sim$800 to $\sim$400 G with the radial distance from the pore. Moreover, the magnetic field inclination in the penumbra-like area is $\sim5^\circ$, nearly horizontal to the surface. Accordingly, we inferred that the pore and penumbra-like structures did not share a common system of magnetic field, because the penumbra-like structures were not connected to the pore and a magnetic gap also existed. Therefore, the magnetic fields in penumbra-like areas probably did not originate from the transformation of the pore's magnetic field, which is different from the usual sunspot evolution (Leka & Skumanich 1998; Schlichenmaier et al. 2010; Jurčák et al. 2014; Murabito et al. 2016). In particular, how to explain that only strong azimuthal fields appeared in the penumbra-like area is the key point of the following analysis.

In Figures 3(a1)–(a3), snapshots of the distributions of the photospheric magnetic fields are presented. Ahead of the path of the moving pore, the magnetic field is very weak. However, when the pore started to move (Figures 3(a2), (a3)), strong horizontal fields ($\geqslant$500 G) appeared at the front side and moved with the pore. Most of the horizontal fields were oriented in circular direction wrapping around the pore as mentioned above. Compared with the horizontal fields, the vertical fields at the front side were fairly weak with a strength less than 100 G during the whole course. Considering its semicircular configuration and, in particular, the synchronous movement with the pore, the enhancement of horizontal magnetic fields is surely not the result of flux emergence.

The distributions of the vertical electric current density can be derived from the horizontal fields by using

$$j_z = \frac{1}{\mu_0}(\nabla\times\boldsymbol{B})_z = \frac{1}{\mu_0}\left(\frac{\partial B_y}{\partial x} - \frac{\partial B_x}{\partial y}\right), \tag{2}$$

where μ_0 is the magnetic permeability of the vacuum. As shown in Figures 3(b1)–(b3), an apparent negative current was building up accompanied by the proper motion of the pore. The current is concentrated in the pore region and moved along with the pore. Based on this picture, we assume that the induced electric current is primarily vertical and the Lorentz force acting on the pore is primarily horizontal. The assumption is additionally justified by the fact that the pore is in vertical equilibrium. The Lorentz force is roughly given by

$$\boldsymbol{F} \approx -j_z(B_y\hat{e}_x - B_x\hat{e}_y). \tag{3}$$

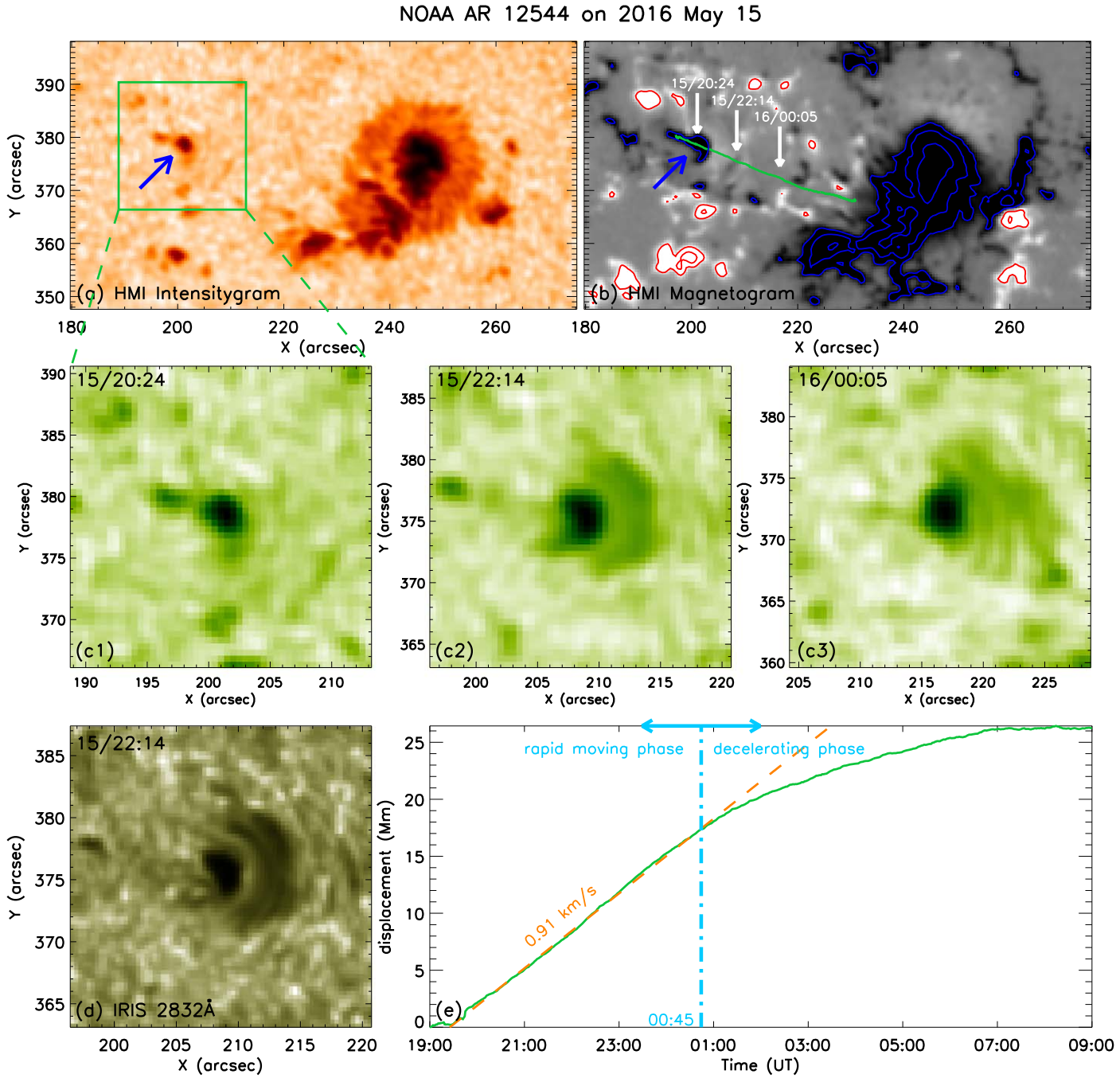

Figure 1. Overview of the rapid moving pore in AR 12544 observed by SDO/HMI. (a), (b) HMI intensity image and line-of-sight magnetogram showing the photospheric conditions, with the target pore highlighted by the blue arrows. The red/blue curves refer to the isogauss contours with levels of ±400, 800, and 1200 G. The green curve shows the trajectory of the pore from 19:00 UT of 2016 May 15 to 09:00 UT of 2016 May 16, and three selected times are marked by the white arrows. (c1)–(c3) Close-up views of HMI intensity images showing the appearance of the penumbra-like structures at the moving front of the pore. The field of view is 24″ × 24″, which is centered on the pore's centroid in each panel. (d) IRIS 2832 Å image showing a clearer view of the pore and penumbra-like structures. (e) Time profile of the displacement of the pore. The vertical dashed blue line marks the time at 00:45 UT of 2016 May 16 to distinguish the rapid moving phase and the decelerating phase of the pore. The dashed orange line is the linear fit to the displacement of the pore in the rapid moving phase, showing the averaged speed is ∼0.91 km s^{-1}. An animation containing panels (a), (b), (c1)–(c3), and (e) is available to show more dynamic details. The animated images run from 2016 May 15 19:00 UT to 2016 May 16 3:00 UT. The video duration is 10 s.

(An animation of this figure is available.)

The results of the distributions of the Lorentz force density calculated by Equation (3) are presented in Figures 3(c1)–(c3). It can be seen that the pore region suffered strong eastward Lorentz forces when moving westward; the Lorentz force is actually acting as a resistance force. In other words, the moving pore was working to overcome the resistance from the induced magnetic fields, in agreement with Lenz's law. As a result, the kinetic energy of the pore could be transformed into the magnetic energy resulting in amplification of the local magnetic fields.

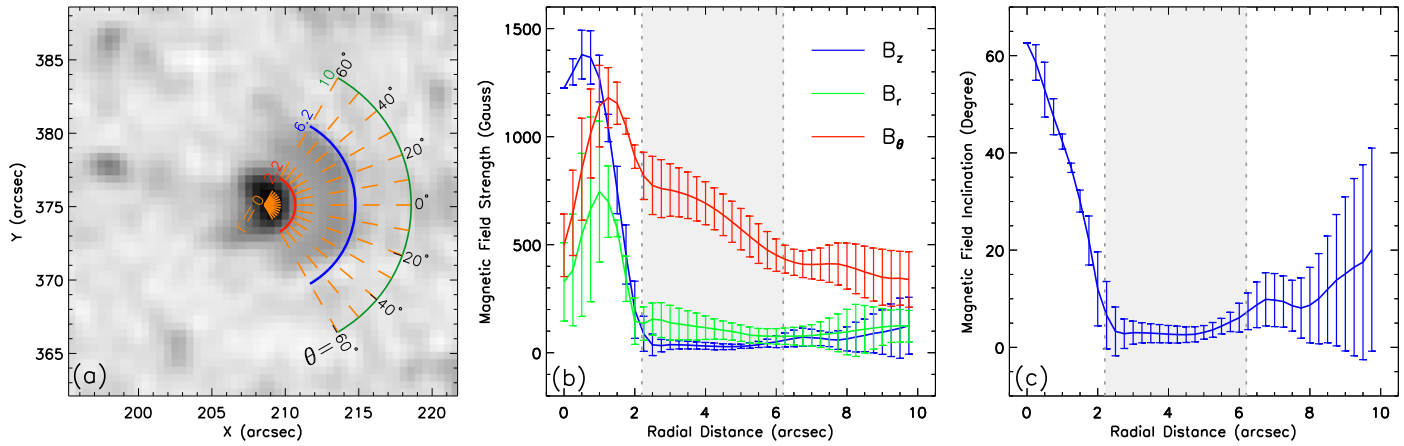

Figure 2. (a) Map of the HMI continuum intensity for the moving pore with semicircular penumbra-like structures. The dashed orange slits are employed to determine the azimuthal averages of the vector magnetic field. The azimuthal angle θ of slits range from $-60°$ to 60° with a cadence of 10°. The red and blue arc curves refer to the inner and outer boundaries of the penumbra-like structures. (b) Azimuthally averaged components of the magnetic field vector as a function of the radial distance r from the sunspot's center. The vertical field B_z is plotted in blue and horizontal field components (B_r, B_θ) are plotted in green and red, which are in the radial and azimuthal directions of the pore, respectively. (c) Azimuthally averaged magnetic inclination with respect to the photospheric surface. In panels (b) and (c), the gray band denotes the region of penumbra-like structures between $r \sim 2\farcs2$ and $6\farcs2$.

3.3. Time Evolutions

To track the temporal evolution of magnetic fields, electric current, and Lorentz force around the pore including its local structures, we use a slice S, which cuts in the east–west direction across the centroid of pore, and two boxes, B1, B2, which cover the compact region of the pore and a larger area around the pore, all moving in pace with the pore. The tracking period was set from 19:00 UT of 2016 May 15 to 03:00 UT of 2016 May 16, covering the whole rapid moving phase and part of the decelerating phase of the pore. The results are presented in Figure 4.

From the spacetime diagram given in (Figure 4(a)), we show that penumbra-like structures started to form at the west side at around 21:40 UT of 2016 May 15. These penumbra-like structures grow up constantly until the pore was approaching the preceding spots and they decayed gradually when the pore was entering the decelerating phase. We see that the appearance of the penumbra-like structures is closely associated with the amplification of the local horizontal fields, which increased about 300 G during the rapid moving phase. The amplification of horizontal magnetic fields mainly occurred at the moving front as shown in Figures 3(a1)–(a3). However, the local vertical fields had no significant change with the mean strength change less than 100 G during the rapid moving phase. It proves again that there was no more magnetic flux emerging from the interior when the pore was under rapid proper motion. Moreover, we can see that the amplification of the local horizontal fields also shows strong temporal correlation with the appearance of the negative current and the enhancement of Lorentz force as presented in Figures 4(b)–(d).

3.4. Amplification of Horizontal Magnetic Fields

All above characteristics strongly suggest a localized amplification of the magnetic field due to the rapid proper motion of the pore. A quantitative verification of this picture can be made via roughly evaluating the amplification through following equation obtained from an ideal MHD induction in an incompressible flow ($\nabla \cdot \boldsymbol{u} = 0$):

$$\left(\frac{\partial}{\partial t} + \boldsymbol{u} \cdot \nabla\right)\boldsymbol{B} = \boldsymbol{B} \cdot \nabla \boldsymbol{u}. \tag{4}$$

Clearly, the left-hand side of Equation (4) is the Lagrangian derivative of $\boldsymbol{B}$ (hereafter referred to as $\frac{D\boldsymbol{B}}{Dt}$), expressing the time rate of change of $\boldsymbol{B}$ following flowing elements, while the right-hand side expresses the fact that the changing rate is proportional to the local shear flows. Considering that the horizontal shear flow driven by the moving pore is more significant in this event, we thus neglect the vertical gradient. After simplification, Equation (4) can be simplified as follows from feasible working equations from observation:

$$\begin{aligned}\frac{DB_x}{Dt} &= B_x\frac{\partial u_x}{\partial x} + B_y\frac{\partial u_x}{\partial y}\\ \frac{DB_y}{Dt} &= B_x\frac{\partial u_y}{\partial x} + B_y\frac{\partial u_y}{\partial y}.\end{aligned} \tag{5}$$

Consequently, the amplification rate of the horizontal magnetic field due to the shear flows can be estimated. Figure 5(a) shows the averaged horizontal flow field ($\overline{u_x}$, $\overline{u_y}$) derived by applying the DAVE4VM method to the HMI vector magnetograms. We track the local shear flows during the time interval from 19:00 UT of 2016 May 15 to 00:48 UT of 2016 May 16, corresponding to the rapid moving phase. These flows were originated from the pore region and moved outward nearly along the radial direction. Many strong flows have a speed $>500\,\mathrm{ms}^{-1}$, concentrated at the moving front.

Then Figure 5(b) gives the magnetic seed fields (B_x, B_y) before being amplified at 20:24 UT of 2016 May 15, as the pore had developed to be stable and was just at the initiation time of the rapid moving phase. Note that the spatial distribution of magnetic fields did not show significant asymmetry at this moment. We use Equation (5) to calculate the growth rate of magnetic field every 12 minutes during the whole rapid moving phase. Figure 5(c) gives the averaged result. It shows that only the magnetic fields at the moving front can be amplified, and more importantly, the generated magnetic

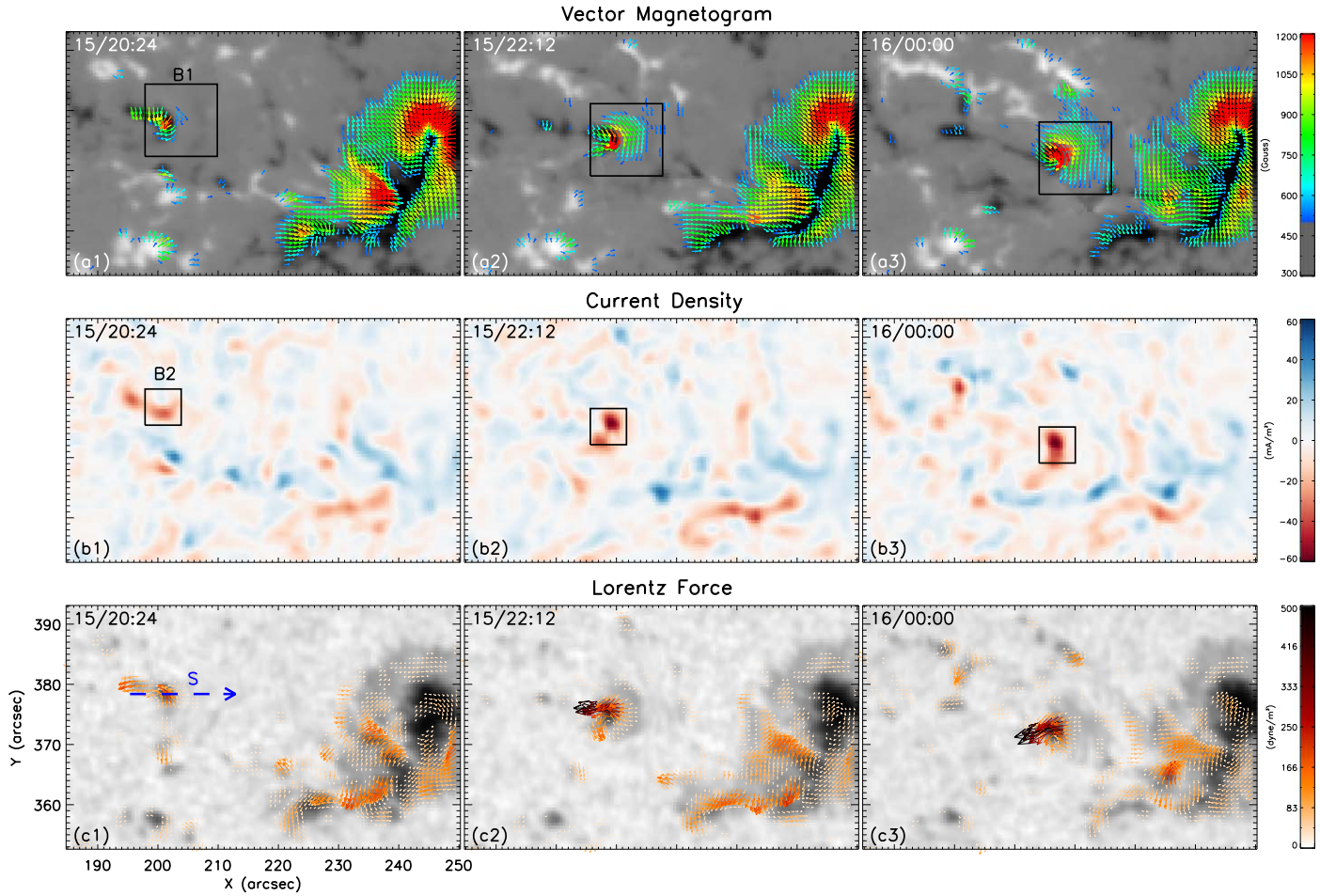

Figure 3. HMI vector magnetograms, the vertical component of the current density j_z, and the Lorentz force density at three different times within the rapid moving duration of the pore. (a1)–(a3) The background gray-scale image shows the vertical field (B_z), and the overplotted arrows represent the horizontal fields ($B_{x,y}$) with color indicating the field strength. (b1)–(b3) The negative and positive currents are defined by the red and blue color scale. (c1)–(c3) Arrows overplotted on the HMI intensity maps represent the photospheric Lorentz forces exerted on the vertical currents, with the length and color indicating the force strength. The boxes (B1 and B2) moving along with the pore mark the regions that are used for further analysis.

fields were oriented in the non-radial direction wrapping around the pore, which was very similar to the observed increasing horizontal magnetic fields as described in Figures 2(b) and 3(a2), (a3). The mean growth rate around the pore (averaged in the black box, the same size as moving box B1) is on the order of ∼15 mG s^{-1}, corresponding to the field's amplification of ∼270 G in 5 hr. The maximum growth rate is on the order of ∼50 mG s^{-1}. Compared with the previous analysis of the magnetograms (Figures 3(a1)–(a3) and 4(b)), the theoretical estimation is well in agreement with the actual observations, thus suggesting that the amplification of horizontal magnetic fields was probably caused by the shear flows driven by the rapid moving pore.

4. Conclusions

Aided by the magnetic field measurements by HMI on board SDO, we analyzed a rapid moving pore in the solar photosphere. When the pore moved toward the preceding spots, ephemeral penumbra-like structures and enhancement of horizontal magnetic fields simultaneously appear in a similar semicircular configuration at the moving front of the pore. It significantly differs from the formation of a partial penumbra around a pore (Schlichenmaier et al. 2010; van Driel-Gesztelyi & Green 2015; Murabito et al. 2018), because the facts are as follows: (1) the penumbra-like structures align in the non-radial direction and are not connected to the pore; (2) a magnetic gap exists between the pore and penumbra-like structures and only a strong azimuthal field can be detected in the penumbra-like area; (3) the penumbra-like structures are unstable and only occur when the pore is under rapid proper motion. All characteristics gathered together let us believe that the formation of penumbra-like structures is a result of the localized magnetic field amplification induced by the rapid moving pore.

By taking the flowing speed and local seed magnetic field detected in the front area of the pore into the MHD induction equation reasonably simplified for this case, the results are in agreement with the observations. In particular, it can account for the unusual phenomenon that only a strong strong azimuthal field is generated in a penumbra-like area. Moreover, the amplification of the horizontal magnetic fields was further associated with the enhancement of the vertical electric current and the Lorentz force exerted on the pore in the inverse direction of the pore's motion, in agreement with Lenz's law. It shows that the vertical electric current was the induced current when the pore was cutting its way through the amplified magnetic field.

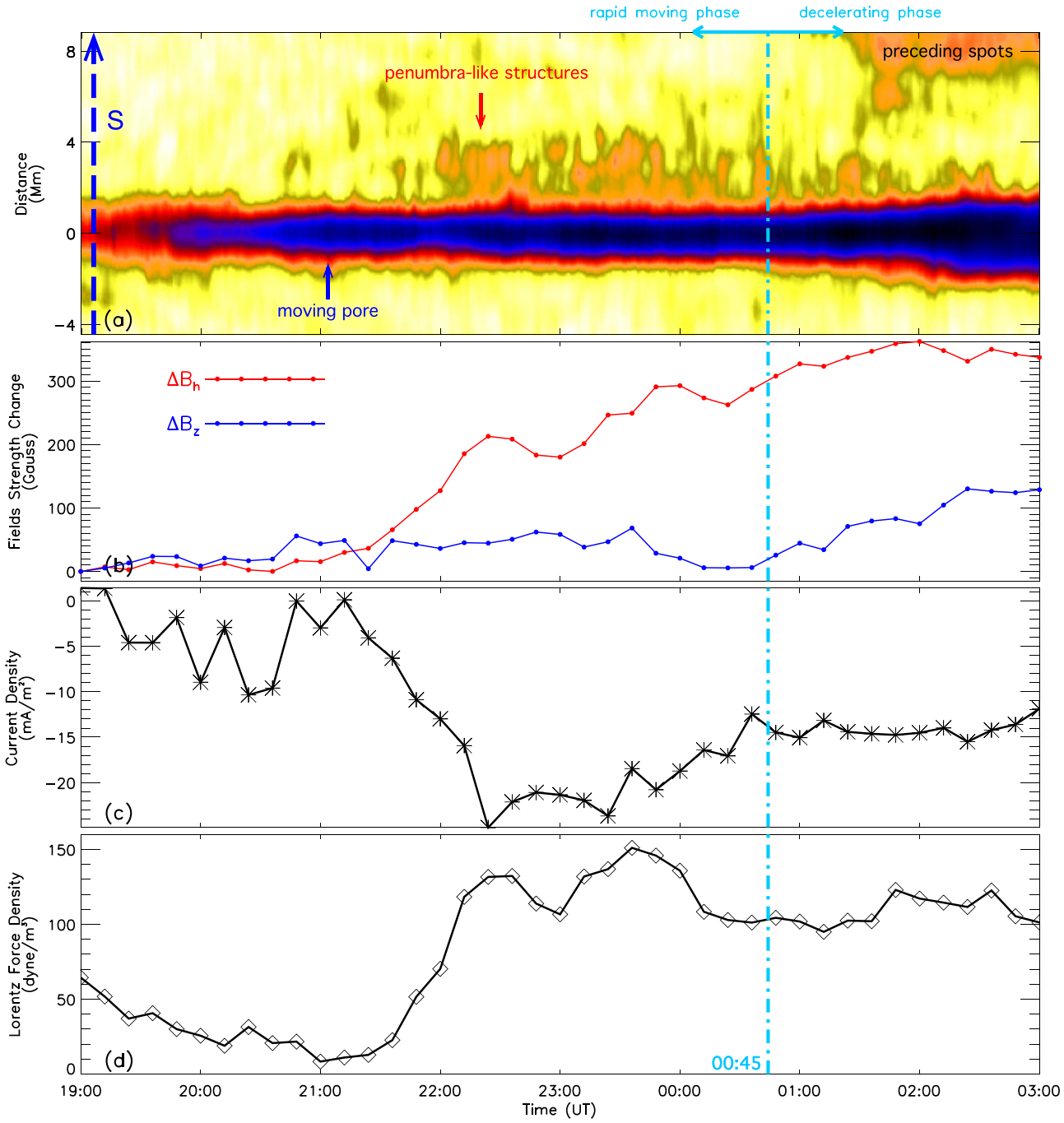

Figure 4. Time evolutions associated with the pore during the whole moving phase and part of the decelerating phase. (a) Time slice from the HMI intensity images for the S slit depicted in Figure 2(c1) shows the evolution of the local structures of the pore. (b) Time profile of the mean strength change of the magnetic field in moving box B1 depicted in Figures 2(a1)–(a3) shows the amplification of the local magnetic fields in the photosphere, with the blue and red curves denoting the strength change of the vertical and horizontal magnetic fields, respectively. (c), (d) Time profiles of the mean electric current density and the Lorentz force density in moving box B2 depicted in Figures 2(b1)–(b3) show the the evolutions of the electric current and the Lorentz force exerted on the pore. The vertical dashed blue line in each panel marks the time at 00:45 UT of 2016 May 16 to distinguish the two phases of motion of the pore.

Consequently, the physical picture of the dynamic process in this case can be drawn clearly. When the buoyant magnetic flux rises from the convection zone to the solar surface, magnetic upflows must expand horizontally to maintain rough pressure equilibrium with its surroundings. In the photosphere, we can see a pore under rapid proper motion after it appears. The proper motion of the pore further drives the ambient magnetic plasma to move radially outward. These outward flows can then amplify the local magnetic fields, which manifested as the significant enhancement of the non-radial horizontal magnetic fields in the front of the pore. As a result, many penumbra-like structures are created because the local convective heat transportation is suppressed by the strong horizontal magnetic fields. On the other hand, the growing ambient magnetic fields can also react to the flux tube of the pore, which inducts an obvious vertical electric current inside the pore. Simultaneously, the pore will suffer a Lorentz force, acting as resistance from the ambient magnetic fields. Via the interaction

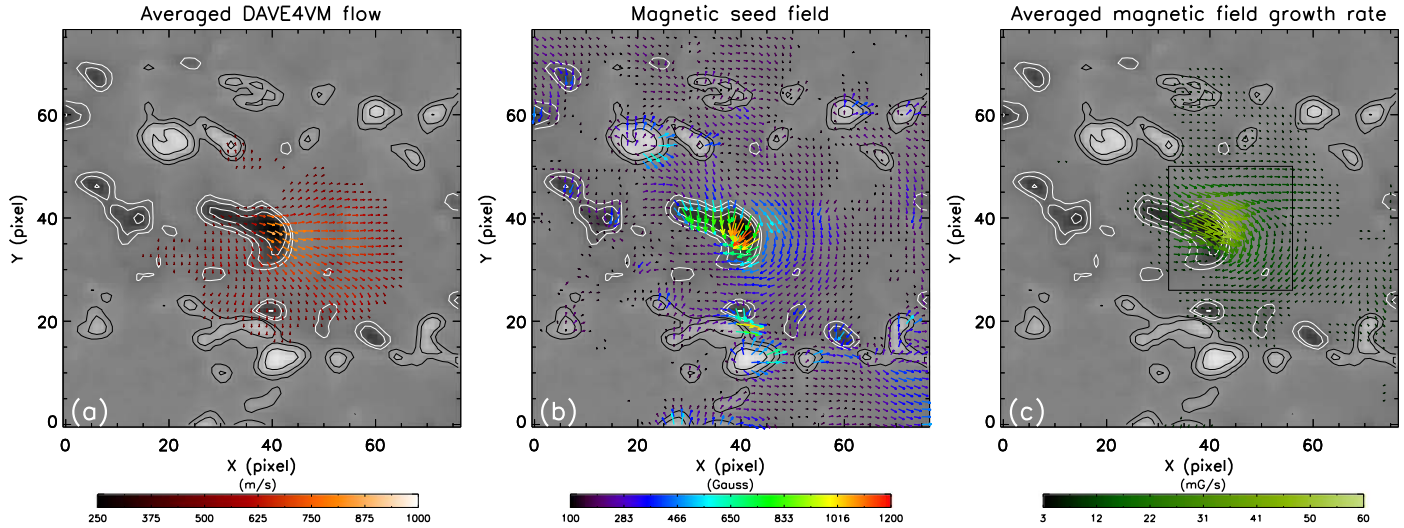

Figure 5. Physical nature of the amplification of the horizontal fields at the moving front of the pore. (a) Local DAVE4VM flow around the moving pore averaged from 19:00 UT of 2016 May 15 to 00:48 UT of 2016 May 16. (b) Magnetic seed field taken from the HMI vector magnetograms at 20:24 UT of 2016 May 15, when the pore was at the initiation time of the rapid moving phase. (c) Magnetic field growth rate averaged from 19:00 UT of 2016 May 15 to 00:48 UT of 2016 May 16, which was estimated based on the ideal MHD induction equation.

between the moving pore and ambient magnetic fields, the kinetic energy of the pore can transfer to the magnetic energy in the photosphere, which leads to the amplification of local magnetic fields.

However, the above scenario is just our conjecture to explain the formation of the unusual penumbra-like structure in this event. Due to the limitations of the data, we cannot observe the solar magnetic field completely and accurately. To confirm our idea, more observational cases and MHD simulations are needed in future work.

The authors thank the referee for many valuable comments that helped improve this article. We thank the SDO and IRIS teams for providing data. This work uses the DAVE/DAVE4VM codes written and developed by P. W. Schuck at the Naval Research Laboratory. Z.X. is grateful for the hospitality of Yunnan Observatories during a visit in 2019 September. This work is supported by the the National Key R&D Program of China (2019YFA0405000), and the Project funded by China Postdoctoral Science Foundation 2020M671639, and the Natural Science Foundation of China under grants 11790302, 11703084, 11773072, 11873088, 11933009, and the Strategic Priority Research Program of Chinese Academy of Sciences, grant No. XDB 41000000.

ORCID iDs

Zhe Xu https://orcid.org/0000-0002-9121-9686
Kaifan Ji https://orcid.org/0000-0001-8950-3875
Yi Bi https://orcid.org/0000-0002-5302-3404
Junchao Hong https://orcid.org/0000-0002-3804-7395
Jiayan Yang https://orcid.org/0000-0003-3462-4340

References

Babcock, H. W. 1961, ApJ, 133, 572
Bobra, M. G., Sun, X., Hoeksema, J. T., et al. 2014, SoPh, 289, 3549
Borrero, J. M., & Ichimoto, K. 2011, LRSP, 8, 4
Brandenburg, A. 2005, ApJ, 625, 539
Brandenburg, A., Jennings, R. L., Nordlund, Å., et al. 1996, JFM, 306, 325
Brandenburg, A., Sokoloff, D., & Subramanian, K. 2012, SSRv, 169, 123
Cameron, R. H., Dikpati, M., & Brandenburg, A. 2017, SSRv, 210, 367
Cattaneo, F. 1999, ApJL, 515, L39
Charbonneau, P. 2014, ARA&A, 52, 251
de Pontieu, B., Title, A. M., Lemen, J. R., et al. 2014, SoPh, 289, 2733
Ermolli, I., Cristaldi, A., Giorgi, F., et al. 2017, A&A, 600, A102
Golub, L., Rosner, R., Vaiana, G. S., et al. 1981, ApJ, 243, 309
Hale, G. E. 1908, ApJ, 28, 315
Jiang, J., Cameron, R. H., & Schüssler, M. 2014, ApJ, 791, 5
Jurčák, J. 2011, A&A, 531, A118
Jurčák, J., Bello González, N., Schlichenmaier, R., et al. 2014, PASJ, 66, S3
Käpylä, P. J., Käpylä, M. J., & Brandenburg, A. 2018, AN, 339, 127
Kitiashvili, I. N., Kosovichev, A. G., Mansour, N. N., et al. 2015, ApJ, 809, 84
Kumar, R., Jouve, L., & Nandy, D. 2019, A&A, 623, A54
Kusano, K., Maeshiro, T., Yokoyama, T., & Sakurai, T. 2002, ApJ, 577, 501
Leighton, R. B. 1969, ApJ, 156, 1
Leka, K. D., & Skumanich, A. 1998, ApJ, 507, 454
Liu, Y., & Schuck, P. W. 2012, ApJ, 761, 105
Murabito, M., Romano, P., Guglielmino, S. L., et al. 2016, ApJ, 825, 75
Murabito, M., Zuccarello, F., Guglielmino, S. L., et al. 2018, ApJ, 855, 58
Parker, E. N. 1955, ApJ, 122, 293
Parker, E. N. 1970, ApJ, 160, 383
Pesnell, W. D., Thompson, B. J., & Chamberlin, P. C. 2012, SoPh, 275, 3
Rempel, M. 2018, ApJ, 859, 161
Rempel, M., & Schlichenmaier, R. 2011, LRSP, 8, 3
Ribes, E., Mein, P., & Mangeney, A. 1985, Natur, 318, 170
Schlichenmaier, R., Rezaei, R., Bello González, N., et al. 2010, A&A, 512, L1
Schou, J., Scherrer, P. H., Bush, R. I., et al. 2012, SoPh, 275, 229
Schuck, P. W. 2008, ApJ, 683, 1134
Turmon, M., Jones, H. P., Malanushenko, O. V., & Pap, J. M. 2010, SoPh, 262, 277
van Driel-Gesztelyi, L., & Green, L. M. 2015, LRSP, 12, 1
Verma, M., Denker, C., Balthasar, H., et al. 2016, A&A, 596, A3
Vögler, A., & Schüssler, M. 2007, A&A, 465, L43